



Original article

Rapid discovery of a novel “green” and natural GST inhibitor for sensitizing hepatocellular carcinoma to Cisplatin by visual screening strategy



Linxi Mao^{a,1}, Yan Qin^{a,b,***,1}, Jialong Fan^b, Wei Yang^c, Bin Li^a, Liang Cao^a, Liqin Yuan^d, Mengyun Wang^a, Bin Liu^{b,**}, Wei Wang^{a,*}

^a TCM and Ethnomedicine Innovation & Development International Laboratory, School of Pharmacy, Hunan University of Chinese Medicine, Changsha, 410208, China

^b College of Biology, Hunan University, Changsha, 410082, China

^c College of Foreign Languages, Hunan Women's University, Changsha, 410004, China

^d Department of General Surgery, The Second Xiangya Hospital, Central South University, Changsha, 410011, China

ARTICLE INFO

Article history:

Received 27 August 2023

Received in revised form

24 November 2023

Accepted 16 December 2023

Available online 21 December 2023

Keywords:

GST

Drug resistance

Fluorescence

Hepatocarcinoma

Natural compound C1

“Green” GST inhibitor

ABSTRACT

Over-expression of glutathione S-transferase (GST) can promote Cisplatin resistance in hepatocellular carcinoma (HCC) treatment. Hence, inhibiting GST is an attractive strategy to improve Cisplatin sensitivity in HCC therapy. Although several synthesized GST inhibitors have been developed, the side effects and narrow spectrum for anticancer seriously limit their clinical application. Considering the abundance of natural compounds with anticancer activity, this study developed a rapid fluorescence technique to screen “green” natural GST inhibitors with high specificity. The fluorescence assay demonstrated that schisanlactone B (hereafter abbreviated as C1) isolated from *Xue tong* significantly down-regulated GST levels in Cisplatin-resistant HCC cells *in vitro* and *in vivo*. Importantly, C1 can selectively kill HCC cells from normal liver cells, effectively improving the therapeutic effect of Cisplatin on HCC mice by down-regulating GST expression. Considering the high GST levels in HCC patients, this compound demonstrated the high potential for sensitizing HCC therapy in clinical practice by down-regulating GST levels.

© 2023 The Authors. Published by Elsevier B.V. on behalf of Xi'an Jiaotong University. This is an open access article under the CC BY-NC-ND license (<http://creativecommons.org/licenses/by-nc-nd/4.0/>).

1. Introduction

Glutathione S-transferase (GST) belongs to the glutathione (GSH)-dependent cellular enzyme system, which plays an important role in the process of drug detoxification and metabolism [1,2]. Growing evidence has indicated that GST over-expression is mainly responsible for drug inactivation and resistance [3–5]. This enzyme can catalyze the binding of GSH to various electrophilic drugs, thereby changing their polarity and enhancing their efflux, leading to greatly reduced drug toxicity [6,7]. Particularly, Cisplatin undergoes extensive detoxification by GST, which leads to drug inactivation, elimination, and resistance [8]. Moreover, GSH easily

couples with these electrophilic drugs and their metabolites when exposed to high levels of GST [9], which is commonly over expressed in cancer cells, such as hepatocellular carcinoma (HCC) [10]. In theory, effective GST inhibition could sensitize the therapeutic effect of Cisplatin in clinical HCC therapy. Therefore, developing GST-targeted inhibitors can improve drug sensitivity in HCC therapy.

Up to now, several GST inhibitors, such as GSH analogs (TLK117/119 and UrPhg/(Et)₂), 6-(7-nitro-2,1,3-benzoxadiazol-4-ylthio)hexanol (NBDHEX) and ethacrynic acid (EA) analogs derived from chemical synthesis and microorganisms, have been reported [11–13]. Among them, NBDHEX has been used in combination with Cisplatin for cancer therapy [14–17]. However, despite being a GST P1-1 inhibitor, NBDHEX showed limited inhibitory effect on other GST sub-types and potential side effects [18–21]. EA was once considered an effective GST inhibitor for clinical application by sensitizing cancer cells to drugs [22,23]. However, the large doses required and long-term usage of EA were found to lead to electrolyte disorders and subsequent fluid imbalance, thereby limiting

* Corresponding author.

** Corresponding author.

*** Corresponding author.

E-mail addresses: 410892672@qq.com (Y. Qin), binliu2001@hotmail.com (B. Liu), wangwei402@hotmail.com (W. Wang).

¹ Both authors contributed equally to this work.

clinical efficacy [24,25]. Hence, developing “green” natural GST inhibitors holds clinical significance.

This study developed a new strategy enabling the rapid discovery of ideal GST inhibitors from natural compounds [26]. As shown in Scheme 1, a smart fluorescent probe (PM) was designed as a powerful “weapon” for discovering “green” GST inhibitors, and further monitoring their regulatory ability on GST levels *in vitro* and *in vivo*. The natural compound schisanlactone B (hereafter abbreviated as C1) isolated from the traditional Chinese medicine (TCM) named *Xue tong* was selected as a potent “green” GST inhibitor. The compound exhibited strong GST inhibition effects both in Cisplatin-sensitive (HepG2) and resistant (HepG2/DDP) HCC cells, while showing high safety to normal hepatocytes with low GST levels. Moreover, compared with Cisplatin monotherapy, the combination of C1 with Cisplatin demonstrated an additive anti-HCC effect on two HCC cell lines and HCC tumor-bearing mice. Considering the high levels of GST in the blood samples of HCC patients, C1 may be a potent drug for HCC treatment in clinical practice. In conclusion, the probe PM was used as a powerful “weapon” to identify GST inhibitors from natural compounds, which can enhance the therapeutic efficacy of Cisplatin on HCC by down-regulating GST levels. This work highlighted the potential of the natural GST inhibitor C1 for clinical HCC treatment with platinum drug resistance.

2. Experimental

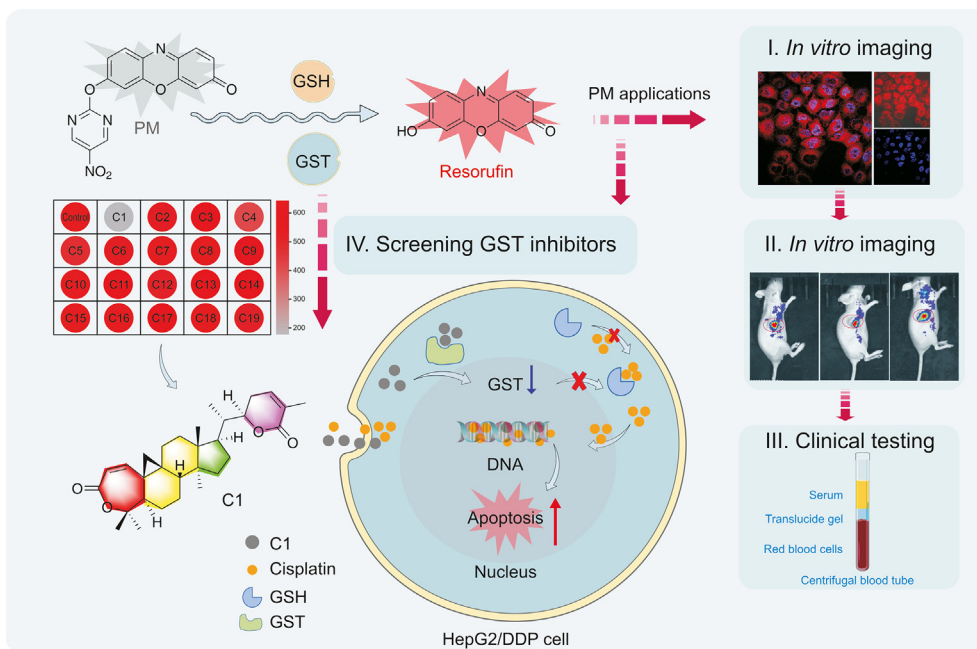
2.1. Materials and reagents

Biological reagents, including GST enzymes (GST, a complex of multiple isoenzymes), Cisplatin, and GSH, were purchased from Sigma Aldrich Chemical Co. (St. Louis, MO, USA) and Shanghai yuanye Bio-Technology Co., Ltd. (Shanghai, China). Pyridine and EA were purchased from Sinopharm (Beijing, China), and Selleck (Houston, Texas, USA), respectively. *N*-Ethylmaleimide (NEM), *N,N*-Dimethylformamide (DMF), dimethyl sulfoxide (DMSO), resorufin, and 2-chloro-5-nitropyrimidine were purchased from Shanghai

Macklin Biochemical Technology Co., Ltd. (Shanghai, China). Phosphate buffer saline (PBS), fetal bovine serum (FBS), Dulbecco's modified Eagle medium (DMEM), trypsin, and methyl thiazolyl tetrazolium (MTT), were purchased from Procell Life Science & Technology Co., Ltd. (Wuhan, China). Annexin V-FITC apoptosis detection kit and BCA protein assay kit were purchased from Beijing Solarbio Science & Technology Co., Ltd (Beijing, China). GST assay kit and GST monoclonal antibodies (glutathione S-transferase class-mu 26 kDa isozyme) were purchased from Nanjing Jiancheng Bioengineering Institute (Nanjing, China), and Abbkine Scientific Co., Ltd. (Wuhan, China), respectively. The reactive oxygen species (ROS) assay kit, 4% paraformaldehyde (PFA), Hoechst 33342, 4', 6-diamidino-2-phenylindole (DAPI), and radioimmunoprecipitation (RIPA) lysate were purchased Beyotime (Nanjing, China). β -actin (1:3,000), Bcl-2 monoclonal antibodies, Bax monoclonal antibodies, caspase 3/p17/p19 monoclonal antibodies and cytochrome C monoclonal antibodies were purchased from proteintech (Wuhan, China). Terminal-deoxynucleotidyl transferase-mediated nick end labeling (TUNEL) and 3, 3'-diaminobenzidine (DAB) dyeing were purchased from Elabscience Biotechnology Co., Ltd. (Wuhan, China). The cells were purchased from FuHeng Biology (Shanghai, China). Natural compounds isolated from *Xue tong* were provided by the TCM and Ethnomedicine Innovation & Development International Laboratory of Hunan University of Chinese Medicine.

2.2. Apparatus

Fluorescence and spectra were measured on the F-7000 spectrophotometer (Hitachi, Ltd., Tokyo, Japan) and UV-1800 ultraviolet spectrophotometer (Shimadzu Co., Ltd., Tokyo, Japan), respectively. Fluorescence imaging was performed by confocal microscopy (FV 1200, object lens: 60 \times and 20 \times ; Olympus Corporation, Tokyo, Japan). Apoptosis analysis was carried out on the flow cytometer (Dakewe Biotech Co., Ltd., Shenzhen, China). High performance liquid chromatography (HPLC) data was obtained by



Scheme 1. Schematic illustration for schisanlactone B (C1) screening and anti-hepatocellular carcinoma (HCC) study. (I–III) Synthesis and application of a smart fluorescent probe (PM). (IV) The potential application of C1 to the regulation of glutathione S-transferase (GST) levels. GSH: glutathione.

high performance liquid chromatography instrument (Shimadzu). Nuclear magnetic resonance spectroscopy (NMR) results were obtained on NMR spectrometers (600 MHz) (Bruker Corporation, Billerica, Germany). Mass spectrum (MS) was determined by liquid phase mass spectrometry (Thermo Fisher Scientific, Rockford, IL, USA). The MTT data were measured by the microplate detector (PerkinElmer Inc, Waltham, MA, USA). The prepared samples for fluorescence measurement were reacted at 37 °C in a water bath. All plastic articles used in the cell room were sterilized at high temperatures. All the cells were cultured in the CO₂ incubator (HERA CELL 150i) (Thermo Fisher Scientific). All cell experiments were performed in the biosafety cabinet (Thermo Fisher Scientific).

2.3. Synthesis of PM

Resorufin (1 mg), 2-chloro-5-nitropyrimidine (8.8 mg), and pyridine (20 µL) were added in 10 mL DMF and stirred for 8 h under N₂ atmosphere at room temperature. The mixture was extracted with ethyl acetate and saturated salt water. It was purified by silica gel chromatography with petroleum ether and ethyl acetate (2:1, V/V) elution to obtain probe PM (yellow solid, 1.05 mg, 66.47%). ¹H NMR (600 MHz, DMSO-d₆) δ_H 9.50 (s, 2H), 7.97 (d, J = 8.7 Hz, 1H), 7.62 (d, J = 2.5 Hz, 1H), 7.59 (d, J = 9.8 Hz, 1H), 7.42 (dd, J = 8.7, 2.5 Hz, 1H), 6.86 (dd, J = 9.8, 2.1 Hz, 1H), 6.32 (d, J = 2.1 Hz, 1H). Liquid chromatography-mass spectrometry (LC-MS) *m/z*: [M⁺] calculated for C₁₆H₈N₄O₅⁺, 336.0495; measured, 337.1000.

2.4. Spectroscopic measurements

The stock solution of probe PM (1 mM) was dissolved in DMSO/water (1:9, V/V) and GSH was prepared in distilled water. The solution of PM for spectral measurement was diluted with PBS to the final concentration (20 µM). GSH was diluted to different concentrations. The test solutions were reacted at 37 °C for 30 min and all spectroscopic experiments were carried out at room temperature. The fluorescence or UV spectra were recorded after the addition of various analytes. The excitation and the emission wavelength were 500/585 nm, and the emission wavelength ranged from 550 nm to 650 nm.

2.5. Cell culture and MTT assay

HL-7702 (normal human hepatocytes), HepG2, and HepG2/DDP were cultured with DMEM (10% FBS and 100 U/mL/1% streptomycin) at 37 °C in a CO₂ incubator. Cells were seeded in 96 well plates (8 × 10³ cells/well), and different concentrations of PM (0–60 µM), C1 (0–25 µM), and Cisplatin (0–20 µM) were added to the cell culture medium (1% FBS) for 48 h. Subsequently, MTT solution (0.5 mg/mL) was added to each well for another 4 h of incubation, followed by MTT assay.

2.6. Screening of natural GST inhibitors

The natural compounds (C1–C19, 20 µM) and GST (20 µg/mL) were incubated with PBS at room temperature for 30 min, followed by co-incubating with GSH (100 µM) and PM (20 µM) at 37 °C for 30 min with fluorescence assay. For median inhibitory concentration (IC₅₀) testing of natural compounds, C1 and other compounds reacted with GST (20 µg/mL) in the presence of GSH (100 µM), followed by fluorescence measurement.

2.7. Molecular docking

Molecular docking was performed using LeDock. The results were then protonated and the energy of the compound was

minimized to obtain a stable 3D structure. The amino acid sequence of GST (PDB code:1EEM) from NCBI databases was downloaded for molecular docking. PM, GSH, C1, and GST (amino acid sequence) were docked by LeDock software.

2.8. Cell imaging

Cells (8 × 10⁴ cells/well) were cultured in 12-well plates with EA, C1, and Cisplatin for 24 h. Then, the cells were pre-treated with NEM for 30 min and stained with Hoechst 33342 (200 µL) and probe PM (100 µM) for 20 min, followed by fluorescence imaging.

2.9. Western blotting

Cells (1 × 10⁶ cells/well) were cultured in the 6-well plates with EA (10 µM) and C1 (5 µM, 10 µM) treatment for 24 h and harvested. The protein concentration in the total extract was quantitated by the BCA protein assay kit (562 nm). The expression of GST was detected strictly by Western blotting (WB) with different antibodies: β-actin (1:3,000), GST monoclonal antibodies, Bcl-2 monoclonal antibodies, Bax monoclonal antibodies, caspase 3/p17/p19 monoclonal antibodies, and cytochrome C monoclonal antibodies (1:1,000). The detection was carried out on the BIO-RAD ChemiDoc XRS chemiluminescence system (Hercules, CA, USA).

2.10. Flow cytometry, cell cycle arrest, ROS assay, and mitochondrial damage tracking

Cells (1 × 10⁶ cells/well) were cultured in 6-well plates and were treated with C1 (7.5 µM, 10 µM), Cisplatin (5 µM), or a combination of Cisplatin and C1 (5 µM and 7.5 µM) for 48 h. Then, the cells were collected and stained with Annexin V-FITC and propidium iodide (PI) dye in 500 µL of binding buffer in a dark environment for 15 min, followed by flow cytometry apoptosis tests. The cell cycle arrest effects of C1 and Cisplatin on HepG2 and HepG2/DDP cells were analyzed by flow cytometry assay. Cells were treated with C1 (10 µM), Cisplatin (5 µM), and C1/Cisplatin (10/5 µM) for 48 h and then collected and fixed overnight in a 4 °C refrigerator with 70% anhydrous ethanol. The next day, the fixed solution was washed away and the cells were stained using a DNA content quantitative assay (cell cycle) for cell cycle arrest assay. For the ROS assay, the cells were cultured in 6-well plates and treated with C1 (10 µM), Cisplatin (5 µM), and C1/Cisplatin (10/5 µM) for 6 h, and stained by the ROS assay kit for detection. For mitochondrial damage tracking, the HepG2 and HepG2/DDP cells were seeded into 12-well plates (8 × 10⁴ cells/well) with C1, Cisplatin, and C1/Cisplatin for 24 h. Subsequently, the cells were stained with Mito-Tracker Red CMXRos (Beyotime, Nanjing, China) for 30 min, then were fixed with 4% PFA for 15 min and treated with DAPI (200 µL) for 15 min, followed by fluorescence imaging.

2.11. In vivo imaging

BALB/C mice (6–8 weeks, 18–20 g) were provided by Beijing Vital River Laboratory Animal Technology Co., Ltd. (Beijing, China) and randomly divided into five groups (*n* = 3). HepG2 and HepG2/DDP cells (5 × 10⁶ cells in PBS) were injected subcutaneously into the nude mice. When the tumor volumes reached around 80 mm³, the mice were injected *in situ* with the corresponding treatments (C1, EA, Cisplatin), followed by PM injection after 30 min for fluorescence monitoring. The animal study protocol was endorsed by the Animal Research Ethics Committee, Hunan University of Chinese Medicine (Approval No.: LL2022101219).

2.12. Detection of GST levels in clinical samples

The serum samples were collected from the second Xiangya Hospital of Central South University. Clinical serum samples (2 μ L) were mixed with GSH (100 μ M) reacted at 37 $^{\circ}$ C for 30 min, and then used for fluorescence measurement. All spectroscopic experiments were carried out at room temperature. In addition, the serum samples were also detected by a GST assay kit (colorimetric method). All the clinical sample studies were approved by the Second Xiangya Hospital, Central South University (Approval No.: KYLL2018072).

2.13. In vivo antitumor activity assay

HepG2/DDP tumor-bearing nude BALB/C mice (female) were randomly divided into 4 groups ($n = 3$ per group) and injected with PBS, C1 (10 mg/kg), Cisplatin (5 mg/kg), and C1/Cisplatin (5 mg/kg + 2.5 mg/kg) at 2-day intervals for 16 days. Body weight and tumor volume were recorded every 2 days. After comparing the tumor size in different groups, tumor-bearing mice were sacrificed to collect tumors; the tumors were weighed and photographed, and the tumor inhibition rate (TIR) was calculated. Histological analysis and pharmacodynamic analysis were performed using

hematoxylin and eosin (H&E) and TUNEL assay. The tumors were fixed with 4% PFA (24 h) and then sliced into paraffin sections (5 μ m). H&E staining and the TUNEL experiment were performed according to the manufacturer's instructions.

The expression of GST, Bcl-2, Bax, and Cyto C in tumor tissues was detected by immunohistochemistry. The paraffin sections of tumor tissues with different treatments were dewaxed. After acid-base repair, ovalin and D-biotin were added for blocking, and the endogenous peroxidase was blocked with a 3% hydrogen peroxide solution. Then, the prepared primary antibody solutions were added to the slides and incubated for 2 h in a wet box away from light. The reaction enhancement solution was incubated for 20 min in a light-resistant environment, and incubated for 20 min in a dark environment with the secondary antibodies labeled with horseradish peroxidase (HRP) corresponding to the primary antibodies. After DAB dyeing, the nucleus was re-stained with hematoxylin for 5 min. The sections were scanned and sealed under an inverted microscope. WB analysis was performed to detect protein expression levels in tumor tissues. Tumor tissues were broken up by homogenizer and RIPA lysate was added to extract total protein. Blood samples were collected for the biochemical and hematological assays. Meanwhile, the heart, liver, spleen, and kidney were collected for sectioning and H&E staining.

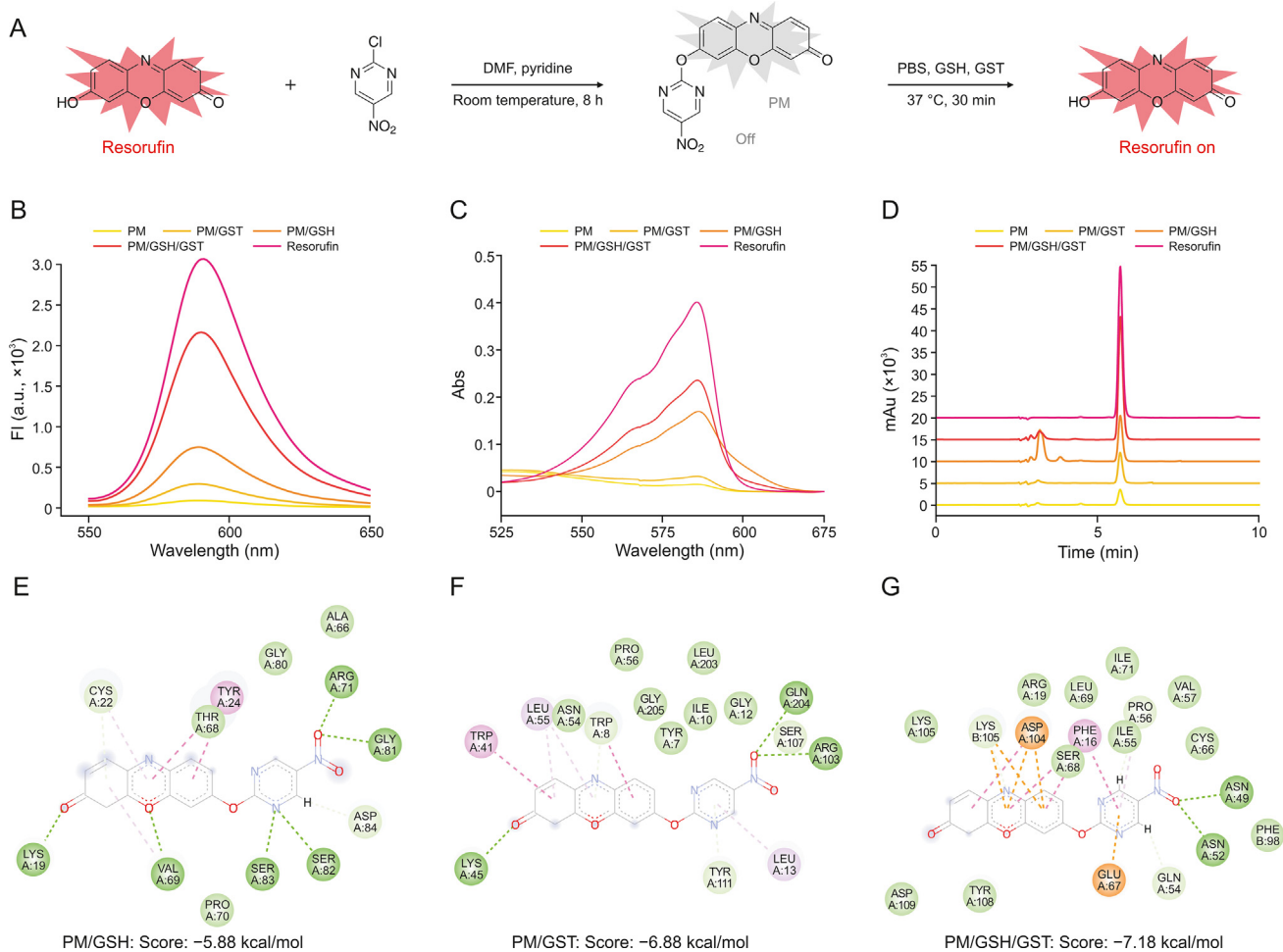


Fig. 1. The feasibility of glutathione S-transferase (GST) detection. (A) The synthesis route of a smart fluorescent probe (PM). (B) Fluorescence emission spectra of PM (20 μ M) in dimethyl sulfoxide (DMSO)/water (1:9, V/V) mixture with different samples at 37 $^{\circ}$ C. (C) Absorption spectra of PM (20 μ M) in DMSO/water (1:9, V/V) mixture with different samples at 37 $^{\circ}$ C. (D) High performance liquid chromatography (HPLC) spectra of PM (20 μ M) in DMSO/water (1:9, V/V) mixture with different samples at 37 $^{\circ}$ C. glutathione (GSH) = 100 μ M, GST = 20 μ g/mL. (E–G) Molecular docking analysis of 2D simulation diagram for PM/GSH (E), PM/GST (F), and PM/GSH/GST (G), respectively. DMF: N,N-Dimethylformamide.

2.14. Safe evaluation of C1 and Cisplatin

All mice received euthanasia at the end of the treatment. Tumors and major organs were harvested and weighed for H&E-staining.

2.15. Statistical analyses

The data were analyzed by GraphPad Prism 9 software and represented as mean \pm standard deviation (SD), $n = 3$ independent experiments. * $P < 0.05$, ** $P < 0.01$, *** $P < 0.001$, while ns represented no statistical significance compared with the vehicle group in the one-way analysis of variance (ANOVA) test.

3. Results and discussion

3.1. Design, synthesis, and cell safety detection of PM

This study is a continuation of our previous finding that resorufin could emit a strong fluorescence signal under suitable wavelength excitation [27]. Resorufin was used as a fluorophore substrate and 2-chloro-5-nitropyrimidine as the fluorescence quencher to construct a new PM probe, which promotes fluorescence resonance energy transfer (FRET) [28–30]. The synthesis process of PM is shown in Fig. 1A, and the data of ^1H NMR and

LC–MS (Fig. S1) confirmed the successful synthesis of PM. Meanwhile, the quantum yield of PM reached about 0.36 (Table S1), which is higher than that of our previously reported probe (0.22) [31]. The nucleophilic reaction and electron transfer between the resorufin moiety and 2-chloro-5-nitropyrimidine moiety resulted in the ultra-low fluorescence signal of PM. In contrast, GST can release the fluorophore of resorufin from PM in the presence of GSH, which is reflected by the increase in fluorescence during the reaction. Furthermore, the high cell viability ($\approx 90\%$) was observed in HL-7702, HepG2, and HepG2/DDP cells after incubating with PM (20 μM) for 24 h (Fig. S2), indicating good cell safety. The probe PM offers a simple synthesis route, a high signal-to-noise ratio (S/N, 10.2) (Table S2), and good safety, and may be expected to be a powerful “weapon” for detecting GST levels.

3.2. Feasibility, specificity and sensitivity of PM for GST detection

The feasibility of the above scheme was evaluated by investigating the spectral properties of PM for GST assay. Fig. 1B illustrates that the weak fluorescence signal of PM at 585 nm was greatly enhanced under GST catalysis in the presence of GSH (PM/GSH/GST). Meanwhile, UV-vis analysis also showed a strong absorption peak of resorufin at 585 nm after the reaction of PM and GSH, catalyzed by GST (Fig. 1C). In addition, the HPLC spectrum showed that the peak of resorufin at 6 min was consistent with that of the

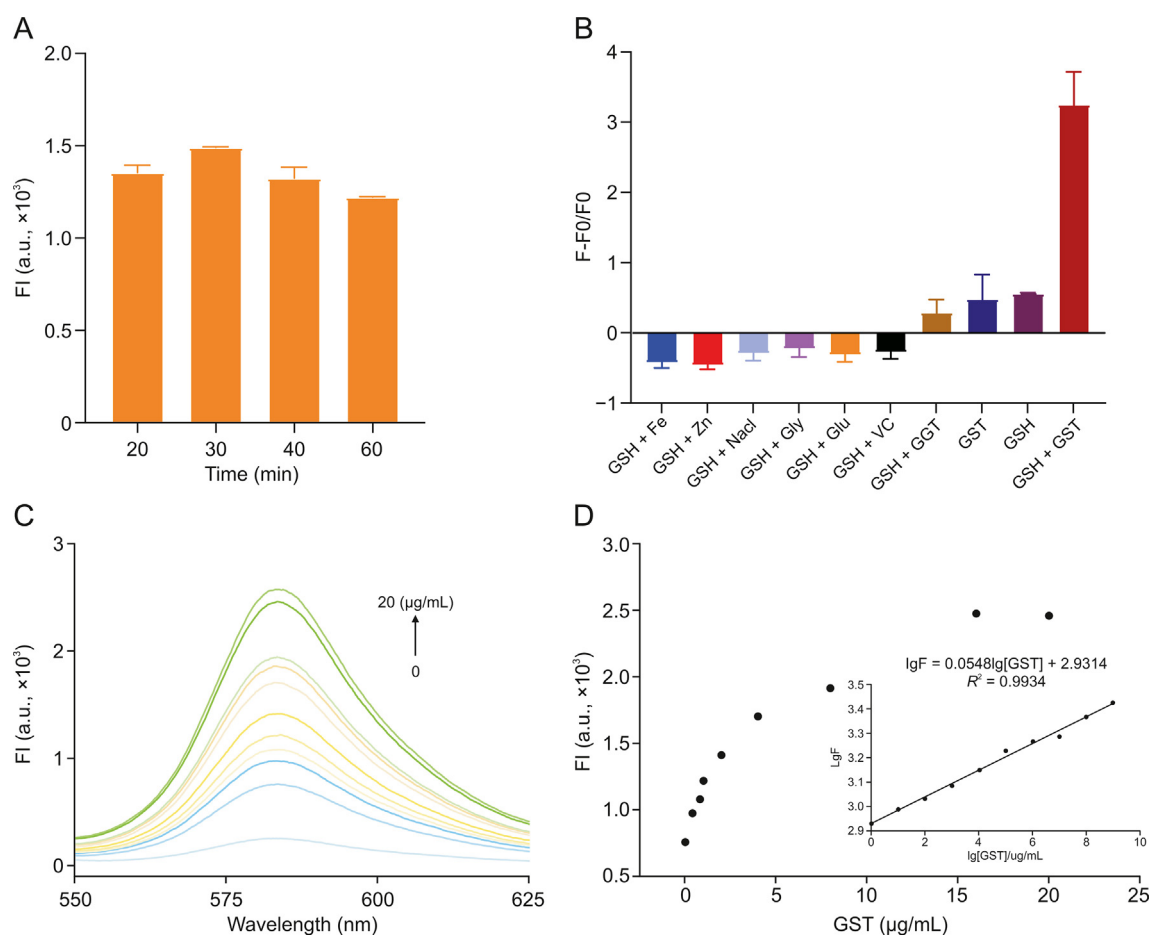


Fig. 2. Specificity and sensitivity of glutathione S-transferase (GST) detection. (A) Optimization of a smart fluorescent probe (PM) reaction time. (B) Specificity response of probe PM in the presence of other interference. PM = 20 μM , glutathione (GSH) = 100 μM , GST = 20 $\mu\text{g/mL}$, interference = 100 μM . (C) Fluorescence spectral of sensitivity assay of GST detection. PM = 20 μM , GSH = 100 μM . (D) The fluorescence intensity (FI) changes of PM to GST and the linear region of GST. Gly: glycine, Glu: glutamic acid, VC: vitamin C, GGT: gamma-glutamyltransferase.

complex (PM/GSH/GST), indicating the release of resorufin from PM under GST catalysis in the presence of GSH (Fig. 1D). Furthermore, molecular docking analysis indicated that the binding free energy gradually decreased in a sequence of PM/GSH binding (Fig. 1E, -5.88 kcal/mol), PM/GST binding (Fig. 1F, -6.88 kcal/mol) and PM/GSH/GST binding (Fig. 1G, -7.18 kcal/mol). The decrease in free energy improved the binding stability and the binding of PM to GST was found to be the most stable in the presence of GSH (PM/GSH/GST), which is beneficial for resorufin release from PM under GST catalysis.

By thoroughly optimizing reactive parameters, the optimal concentrations of PM, GSH, and GST were determined as $20 \mu\text{M}$, $100 \mu\text{M}$, and $20 \mu\text{g/mL}$ (Figs. S3–S5), respectively. Moreover, the detection time was set to 30 min (Fig. 2A). Subsequently, the effect of potential interfering substances on the GST assay was investigated, revealing that PM only exhibited a highly specific response to GST in the presence of GSH. In contrast, other co-existing substances exerted a negligible impact on the GST detection (Fig. 2B). To determine the sensitivity, PM ($20 \mu\text{M}$) was mixed in PBS (pH 7.4) containing various GST concentrations and GSH ($100 \mu\text{M}$) at 37°C for 30 min. The fluorescence signal increased gradually as the GST concentration was increased, which revealed a good linear relationship ($R^2 = 0.9934$) between the fluorescence intensity and GST concentration (Figs. 2C and D). The limit of detection (LOD) ($3\sigma/\text{slope}$) for GST was calculated to be $0.07 \mu\text{g/mL}$, which is comparable with other methods [30–33] (Table S3).

3.3. Natural GST inhibitor screening

Considering the high specificity and sensitivity of the GST detection system, “green” natural GST inhibitors were screened

from TCM compounds (*Xue tong*, 19 natural compounds). C1 was found to inhibit GST activity with an IC_{50} of $5 \mu\text{M}$ (Figs. 3A–C). Moreover, the molecular docking analysis disclosed the inhibitory mechanism of C1 on GST. As shown in Fig. 3D, C1 binds with several amino acids (PROA:73, GLUA: 85) of GST through Van der Waals with a score of -5.38 (kcal/mol), indicating that C1 closely interacts with GST to exert its inhibitory effect. Considering both C1 and probe PM can bind to GST, the effect of C1 on the binding between PM and GST was investigated. Fig. S6 indicated no significant difference in the fluorescence intensity of C1 combined with GST before or after PM. In contrast, Fig. S7 verified that C1 did not directly react with resorufin to affect the fluorescence signal. These results demonstrated a PM-independent binding between C1 and GST.

3.4. Inhibitory effect of C1 on intracellular GST in HCC cells

After verifying the effective inhibition of C1 on extracellular GST activity, the exact intracellular GST inhibitory effect of C1 was accordingly explored in Cisplatin-sensitive and resistant HCC (HepG2 and HepG2/DDP) cells. A gradual decrease in GST levels was observed in the sequence of HepG2/DDP, HepG2, and HL-7702 (Figs. 4A and B). These results clearly indicated that GST levels were higher in cancer cells and exhibited a positive relation between GST levels and Cisplatin resistance in HCC cells. Meanwhile, the difference in GST levels was also investigated in HepG2 and HepG2/DDP cells with different treatments. As shown in Figs. 4C–F, C1 down-regulated GST levels in a concentration-dependent manner both in HepG2 and HepG2/DDP cells. Meanwhile, two other natural compounds (C2 and C3) showed very weak GST inhibitory activity in drug screening results and were

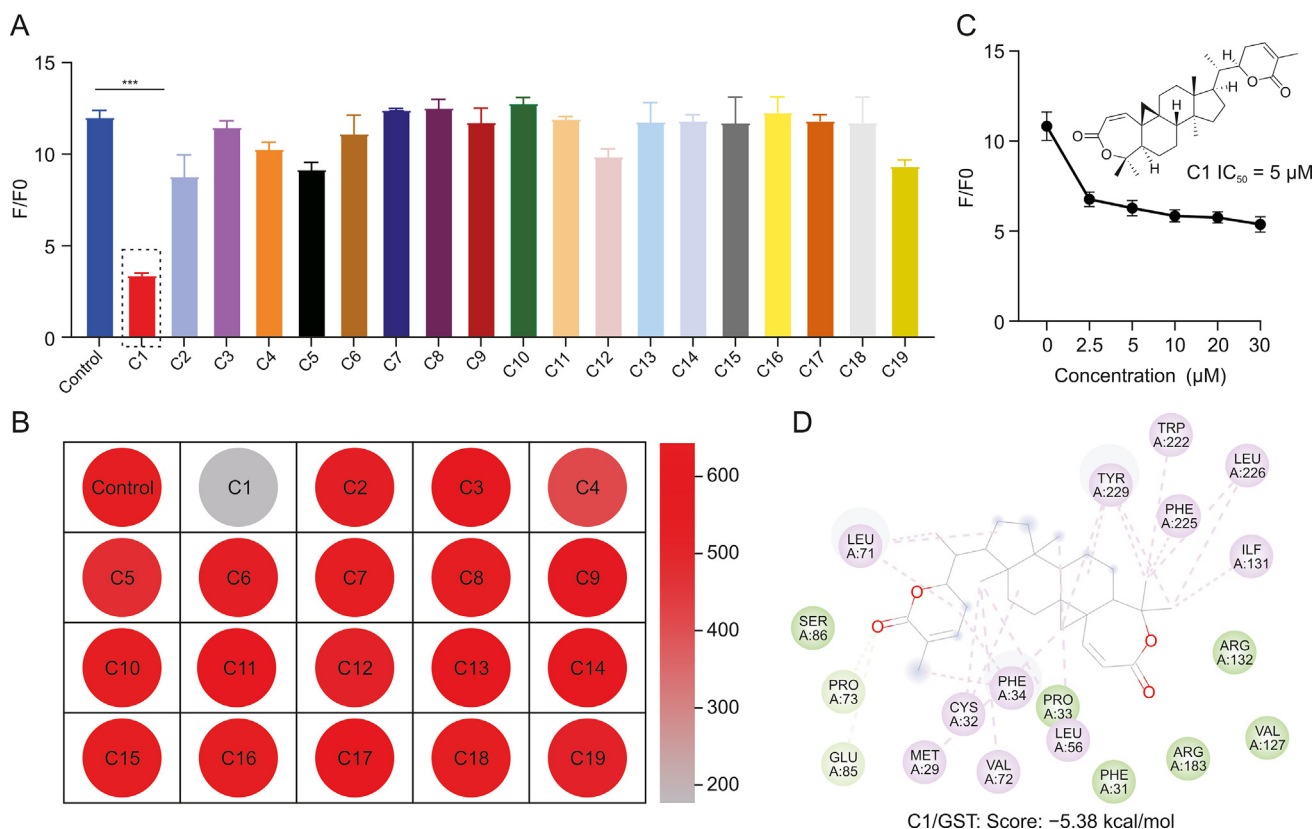


Fig. 3. Glutathione S-transferase (GST) inhibitors screening from natural drugs of *Xue tong*. (A, B) Detection of different natural compounds on GST activity. (C) Detection of schisanlactone B (C1) inhibiting ability on GST. Compounds = $20 \mu\text{M}$, PM = $20 \mu\text{M}$, GST = $20 \mu\text{g/mL}$, glutathione (GSH) = $100 \mu\text{M}$. (D) Molecular docking analysis of 2D simulation diagram for C1 and GST. Error bars denote the standard deviation ($n = 3$), $*P < 0.001$. C1–C19: the compounds is isolated from *Xue tong*.

selected as controls. Expectedly, C1 showed the strongest ability to down-regulate GST levels (Fig. S8). In addition, cell imaging revealed a much weaker red fluorescence after C1 (5 μ M) treatment compared with the negative control (sole PM treatment, 20 μ M), which was comparable to EA (5 μ M) treatment (Figs. 4G and H). These findings indicated the excellent inhibitory ability of C1 on GST in HepG2/DDP cells. Besides, a similar phenomenon was observed in HepG2 cells (Figs. 4I and J). Conclusively, the natural compound C1 exhibited excellent regulatory effects on GST levels in Cisplatin-resistant (HepG2/DDP) and sensitive (HepG2) HCC cells.

3.5. Inhibitory effect of C1 on GST *in vivo*

Moreover, the inhibitory effect of C1 on GST was investigated *in vivo* by using HepG2/DDP and HepG2-bearing BALB/C nude mice subjected to different treatments (PBS, Cisplatin, EA, and C1, administered *in situ* with 5 mg/kg dosage). In the Cisplatin-resistant HCC model (HepG2/DDP), the GST levels kept fluctuating within 0–12 h of C1 injection, as evidenced by the changes in fluorescence intensity (Fig. 5). The fluorescence intensity increased slightly at 8 h compared with 2 h after C1 injection, but then decreased gradually until no obvious fluorescence was observed at

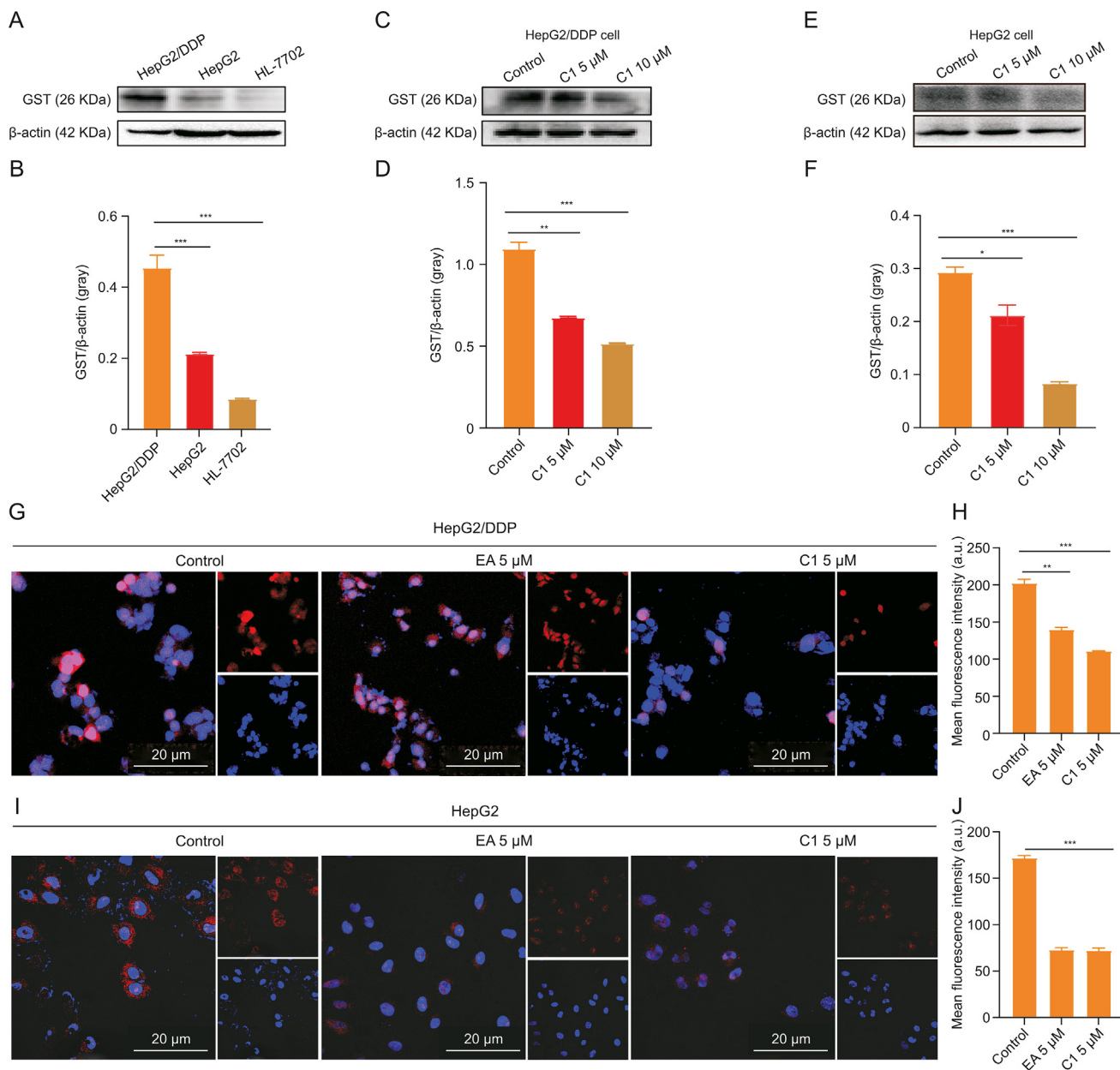


Fig. 4. The Western blotting (WB) analysis and cell imaging of HepG2/DDP and HepG2 cells with different treatments to detect the glutathione S-transferase (GST) expression (A) The protein expression of GST in HepG2/DDP, HepG2, and HL-7702 cells. (B) The quantitative analysis of GST expression in different cells. (C) GST expression in HepG2/DDP cell treated with schisanlactone B (C1) (5, 10 μ M) for 24 h. (D) The quantitative analysis of GST expression in HepG2/DDP cells. (E) GST expression in HepG2 cells treated with C1 (5, 10 μ M) for 24 h. (F) The quantitative analysis of GST expression in HepG2 cells. (G) Cell imaging with different treatments of HepG2/DDP cells for 24 h. C1 = 5 μ M, ethacrynic acid (EA) = 5 μ M. (H) The quantitative analysis of fluorescence intensity in HepG2/DDP cells. (I) Cell imaging with different treatments of HepG2 cells for 24 h. C1 = 5 μ M, EA = 5 μ M. (J) The quantitative analysis of fluorescence intensity in HepG2 cells. Error bars denote the standard deviation ($n = 3$), * P < 0.05, ** P < 0.01, and *** P < 0.001.

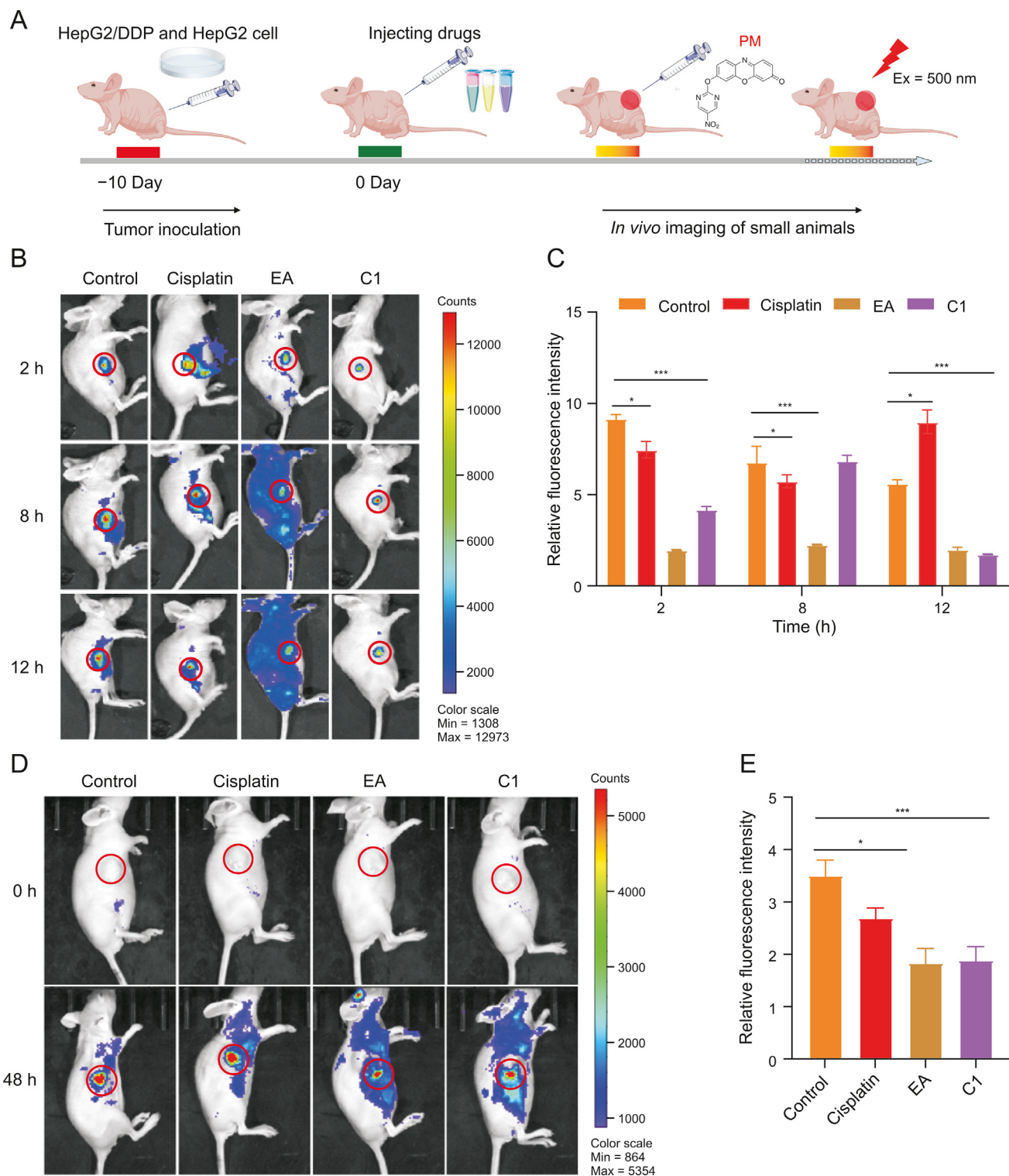


Fig. 5. *In vivo* glutathione S-transferase (GST) tracking of tumor-bearing mice (HepG2/DDP and HepG2). (A) Schematic illustration of *in vivo* imaging. (B) Real-time imaging of different treatment groups in HepG2/DDP tumor-bearing mice. (C) The relative quantitative fluorescence analysis of HepG2/DDP tumor-bearing mice. (D) Real-time imaging of different treatment groups in HepG2 tumor-bearing mice. (E) The relative quantitative fluorescence analysis of HepG2 tumor-bearing mice. Schisanlactone B (C1), ethacrynic acid (EA), and Cisplatin = 5 mg/kg; a smart fluorescent probe (PM) = 20 μM. Error bars denote the standard deviation (n = 3), *P < 0.05, **P < 0.01, and ***P < 0.001.

12 h, which suggested that C1 could regulate GST levels *in vivo* after a period of action time. In addition, C1 and EA showed comparable ability to regulate GST levels. However, relatively strong fluorescence was observed in the control and Cisplatin-treated groups, indicating the negligible effect of Cisplatin on GST levels (Figs. 5B and C). Similarly, in the Cisplatin-sensitive HCC model (HepG2), the fluorescence intensity of the C1-treated group displayed very weak fluorescence compared to the control and Cisplatin groups, which is comparable to that of EA (Figs. 5D and E). Furthermore, WB, fluorescence measurement, and GST assay were performed to detect the GST levels in tumor tissues, yielding results consistent with those of the *in vivo* imaging assay (Fig. S9). Collectively, the natural compound C1 exhibited excellent GST level regulation ability in the HCC model, which might be helpful for enhancing the drug sensitivity in Cisplatin-resistant HCC therapy.

3.6. GST high expression in HCC clinical samples

After confirming the high GST levels in the HCC model *in vitro* and *in vivo*, the difference in GST levels between HCC patients (positive group, $n = 16$) and the normal group (negative group, $n = 16$) was investigated. Fluorescence intensities of serum samples were recorded after the adding of 20 μM PM for 30 min. Although GST levels varied in different clinical samples, the GST average level of the positive group was significantly higher than those of the negative group, as evidenced by the fluorescence intensity (Fig. 6). These results were consistent with those of commercial kit GST assay, confirming the high expression of GST in HCC clinical samples. Considering that GST can serve as an important target for clinical diagnosis and HCC therapy [32], the screened natural GST inhibitor C1 holds great potential clinical application for sensitizing HCC therapy.

3.7. *In vitro* evaluation of C1 enhanced drug sensitivity

Cisplatin inactivation in the refractory and recurrence of cancer is tightly related to high levels of GST [34]. Until now, GST inhibitors have been used to enhance the sensitivity of tumor cells to chemotherapy, but most of them exert self-toxicity and side effects after long-term administration. Considering the strong inhibitory effect of C1 against GST, the sensitizing effect of C1 on the anti-HCC properties of Cisplatin was examined by monitoring the cell viability of HepG2 and HepG2/DDP cells under different conditions. As expected, C1 alone resulted in decreased cell viability in a

concentration-dependent manner both in HepG2 and HepG2/DDP ($\text{IC}_{50} = 17.2 \pm 0.41 \mu\text{M}$ in HepG2, $\text{IC}_{50} = 14.3 \pm 0.45 \mu\text{M}$ in HepG2/DDP). In contrast, Cisplatin monotherapy showed a good anticancer effect in HepG2 ($\text{IC}_{50} = 8.0 \pm 0.35 \mu\text{M}$), but not in HepG2/DDP cells ($\text{IC}_{50} = 80.2 \pm 0.67 \mu\text{M}$) (Figs. S10A and B). Notably, the cytotoxic effect of C1 in HepG2/DDP was slightly stronger than that of HepG2 at the same concentration (Fig. S10C), which might be attributed to the effective inhibitory effect of C1 on GST. In addition, C1 exhibited high safety to normal cell lines (HL-7702, H9C-2, and human umbilical vein endothelial cells (HUVECs)) with cell viability of 85%–95% at 20 μM (Fig. S10D). These results indicated that C1 could selectively target Cisplatin-resistant HCC cells from normal cells, and Fig. S11 showed that there was no significant difference in two experiments (with 1% and 10% FBS culture). In addition, a good additive anti-cancer effect was achieved in HepG2/DDP cells when C1 (7.5 μM –10 μM) was combined with Cisplatin (5 μM –10 μM) (Figs. 7A and S12), which indicated that C1 can sensitize Cisplatin-resistant HCC cells to Cisplatin. Furthermore, the enhanced drug sensitivity effect of C1 was investigated in MCF-7/ADR cells. C1 (5 μM –10 μM) was combined with doxorubicin (DOX) (0 μM –20 μM), yielding good additional anticancer effects and enhancing the killing effect of DOX in DOX-resistant breast cancer cells (MCF-7/ADR). However, DOX monotherapy demonstrated no significant anti-tumor efficacy in MCF-7/ADR (Fig. S13). Besides, the cell cycle assay (Fig. S14) showed that C1 (10 μM) combined with Cisplatin (5 μM) resulted in cell cycle arrest in HepG2 (G2 phase inhibition) and HepG2/DDP (G1 phase inhibition) cells, which confirmed that the drug combination could inhibit tumor growth by affecting the cell cycle.

Flow cytometry assay indicated that C1 induced cell apoptosis in a concentration-dependent manner both in HepG2 and HepG2/DDP cells (Fig. S15). Moreover, 7.5 μM C1 exhibited a slightly stronger ability to induce apoptosis in HepG2/DDP compared to HepG2 (apoptotic rate, 18.9% vs 13.8%). In addition, the apoptotic rate for the combination of Cisplatin with C1 (7.5 μM) was significantly increased compared with Cisplatin (32.82% vs 3.06%) in HepG2/DDP cells (Figs. 7B and C). These results indicated the significant sensitization effect of C1 on Cisplatin-resistant HepG2/DDP cells. In addition, the levels of apoptosis-related proteins were detected, and revealed that Cisplatin and C1/Cisplatin increased the levels of cleaved caspase-3 (C-caspase-3) and Bax, but decreased the expression of (P-caspase 3) and Bcl-2 in HepG2/DDP (Figs. 7D–H). In addition, the ratio of Bax/Bcl-2 and C-caspase-3/P-caspase-3 in C1/Cisplatin (7.5 μM /5 μM)-treated cells increased

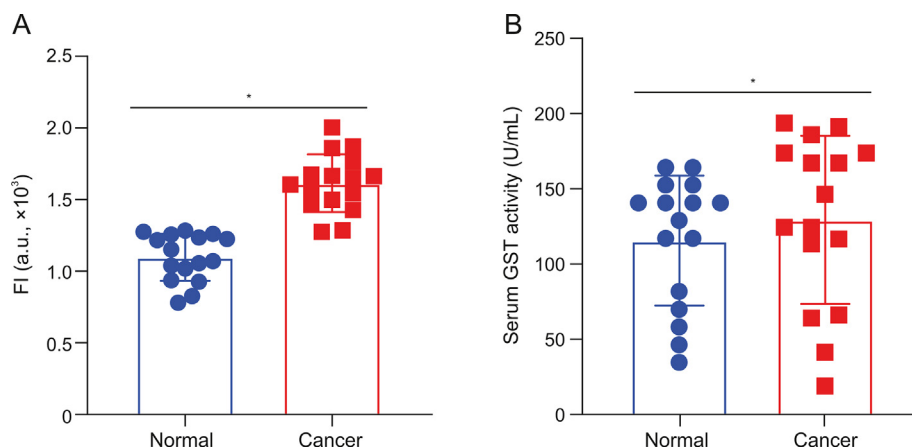


Fig. 6. Glutathione S-transferase (GST) detection of hepatocellular carcinoma (HCC) clinical samples. (A) Fluorescence assay of HCC clinical samples. (B) GST kit assay of HCC clinical samples. The clinical samples were diluted 50-fold for assay. A smart fluorescent probe (PM) = 20 μM , glutathione (GSH) = 100 μM . Error bars denote the standard deviation ($n = 16$), * $P < 0.05$, ** $P < 0.01$, and *** $P < 0.001$. FI: fluorescence intensity.

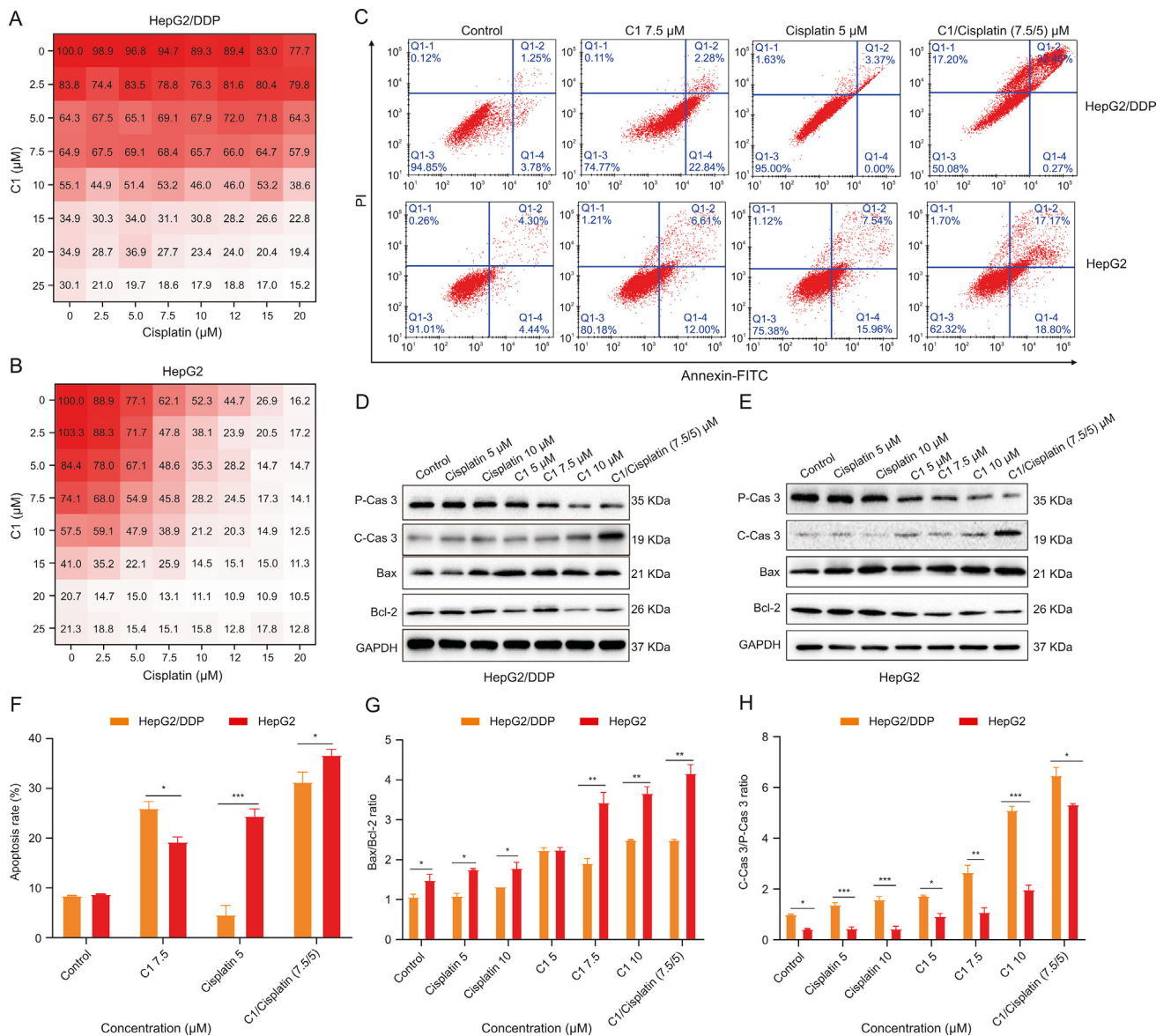


Fig. 7. Potential application of schisanlactone B (C1) in sensitizing Cisplatin therapy. (A, B) The combined anticancer effect of C1 and Cisplatin in HepG2/DDP (A) and HepG2 (B) cells by methyl thiazolyl tetrazolium (MTT). C1 = 0–25 μM, [Cisplatin] = 0–20 μM. (C) Apoptosis analysis with different treatments in HepG2/DDP and HepG2 cells. (D, E) The HepG2/DDP (D) and HepG2 (E) cells treated with Cisplatin (5, 10 μM), C1 (5, 7.5 μM), and combination of Cisplatin and C1 (5, 7.5 μM) to detect the expression of apoptosis-related proteins. (F) Quantitative analysis of the apoptosis rate in HepG2/DDP and HepG2 cells. (G, H) Quantitative analysis of protein expressions in HepG2/DDP and HepG2 cells by Western blotting (WB). Error bars denote the standard deviation ($n = 3$). * $P < 0.05$, ** $P < 0.01$, and *** $P < 0.001$. C-Cas: pro-caspase 3; P-Cas: pro-caspase 3; Bax: Bcl-2-associated X protein; Bcl-2: B-cell lymphoma-2; GAPDH: glyceraldehyde-3-phosphate dehydrogenase.

compared with that of single drug (7.5 μM C1 or 5 μM Cisplatin) in HepG2/DDP cells.

Considering that ROS release and the mitochondrial membrane damage are the most important events of the mitochondrial apoptosis pathway [35], ROS levels and membrane damage were detected to explore the apoptotic pathway. As shown in Figs. 8A and B, C1 combined with Cisplatin produced higher ROS levels than Cisplatin treatment alone both in HepG2 and HepG2/DDP cells. Meanwhile, higher mitochondrial membrane damage was observed with the drug combination compared to Cisplatin monotherapy both in HepG2 and HepG2/DDP, as evidenced by the fading red fluorescence (Figs. 8C–F). Interestingly, mitochondrial membrane damage caused by the drug combination (C1/Cisplatin) was stronger in resistant HCC cells (HepG2/DDP) than in sensitive HCC cells (HepG2). In addition, the drug combination was found to significantly regulate mitochondrial apoptosis (caspase 3, Bax, Bcl-

2) and Cisplatin-resistance (GST) related proteins expression compared with a single drug both in HepG2 and HepG2/DDP (Figs. 8G and H). These changes were accompanied by the release of Cyto C, an important biomarker of mitochondrial apoptosis. The results fully confirmed the Cisplatin sensitization properties of C1 through the mitochondrial apoptotic pathways in Cisplatin-resistant HCC cells.

3.8. Potential application of C1 in sensitization of Cisplatin inactivation in vivo

The enhanced anti-HCC effect of C1 on Cisplatin was investigated using HepG2/DDP tumor-bearing mice. Once the tumors reached 80 mm³, the mice were treated with PBS, C1 (10 mg/kg), Cisplatin (5 mg/kg), and C1/Cisplatin (5 mg/kg + 2.5 mg/kg), respectively (Fig. 9A). Compared with the control group, the

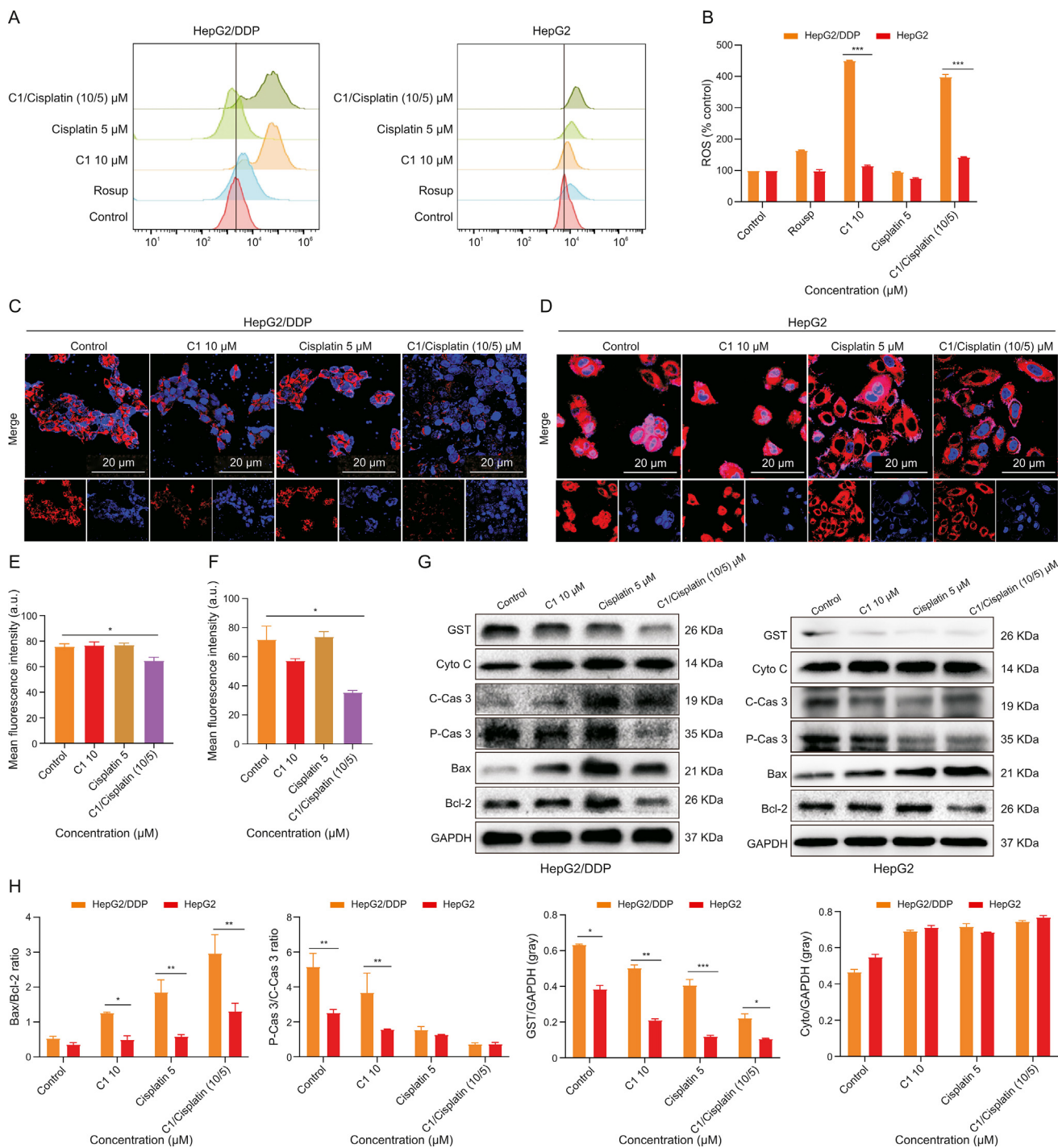


Fig. 8. The reactive oxygen species (ROS) assay, mitochondrial tracking, and Western blotting (WB) detection of HepG2/DDP and HepG2 cells. (A) The cells treated with schisanlactone B (C1) (10 μM), Cisplatin (5 μM), and C1/Cisplatin (10/5 μM) for 6 h to analyze the ROS levels in HepG2/DDP and HepG2 cells. (B) Quantitative analysis of ROS levels in HepG2/DDP and HepG2 cells. (C, D) The cells treated with C1 (10 μM), Cisplatin (5 μM), and C1/Cisplatin (10/5 μM) for 24 h for mitochondrial tracking by using Mito-Tracker Red CMXRos (200 nM, 30 min). (E, F) The quantitative analysis of the mitochondria expression in HepG2/DDP (E) and HepG2 (F) cells. (G) Apoptosis protein expression assay by WB analysis with different treatment. (H) The expression ratio of Bcl-2-associated X protein (Bax)/B-cell lymphoma-2 (Bcl-2), pro-caspase 3 (P-Cas)/cleaved-caspase 3 (C-Cas), and glutathione S-transferase (GST)/glyceraldehyde-3-phosphate dehydrogenase (GAPDH), respectively. Error bars denote the standard deviation ($n = 3$), * $P < 0.05$, ** $P < 0.01$, and *** $P < 0.001$. Cyto C: cytochrome C.

tumor growth in the PBS, C1 (10 mg/kg), Cisplatin (5 mg/kg), and C1/Cisplatin (5 mg/kg + 2.5 mg/kg) groups was suppressed to different degrees. Notably, C1/Cisplatin required only half the dose of C1 and Cisplatin, yielding a stronger therapeutic effect than given alone. *In vitro* photographs and quantitative tumor weight analysis (Figs. 9B–D) directly showed that the C1/

Cisplatin group significantly inhibited tumor growth. As shown in Fig. 9E, the tumor inhibition rates of C1, Cisplatin, and C1/Cisplatin after treatment were 19.4%, 57.8% and 71.7%, respectively. To further investigate the antitumor effects at the tissue and cell level, a histopathological analysis of the extracted tumors was performed. After H&E staining, the tumor sections in

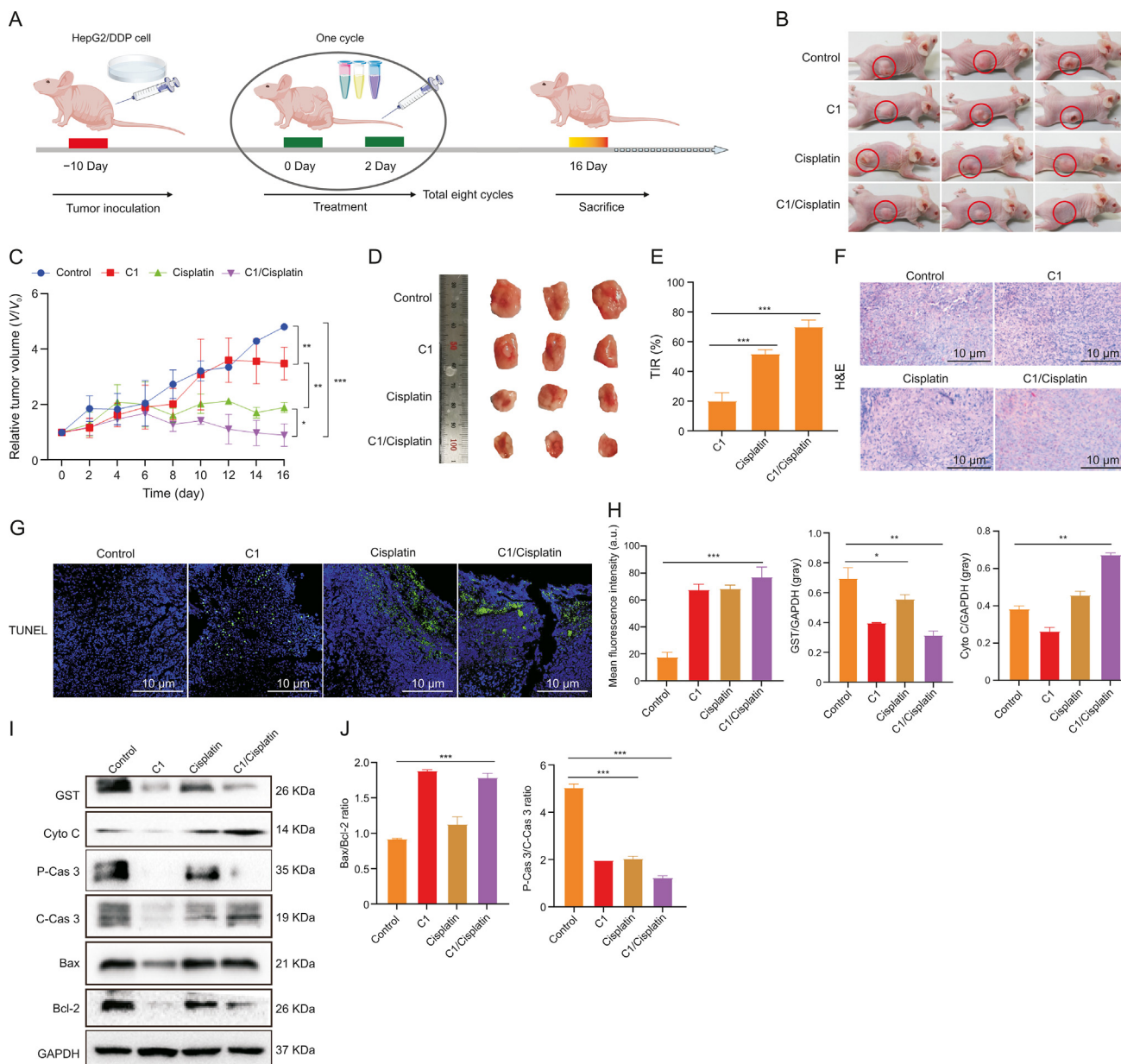


Fig. 9. The enhanced anti-hepatocellular carcinoma (HCC) effects of schisanlactone B (C1) on Cisplatin in HepG2/DDP tumor-bearing mice. (A) Schematic illustration of treatment with nude mice model. (B) The images of HepG2/DDP tumor-bearing mice with different treatments. (C) The relative volume of tumors compared to that of control. (D) The tumor images of different groups. (E) The tumor inhibition rate (TIR) of different groups compared to that of control. (F) Hematoxylin and eosin (H&E) staining images of tumor with different treatments. (G) The TUNEL analysis of tumors after different treatments. (H) The terminal-deoxynucleotidyl transferase-mediated nick end labeling (TUNEL) fluorescence quantification in different groups. (I) Western blotting (WB) analysis of the expression of caspase 3, B-cell lymphoma-2 (Bcl-2), Bcl-2-associated X protein (Bax), glutathione S-transferase (GST), and cytochrome C (Cyto C) in HepG2/DDP tumor-bearing mice of different groups. (J) Quantitative analysis of caspase 3, Bcl-2, Bax, GST, and Cyto C expression in HepG2/DDP tumor tissue. Error bars denote the standard deviation ($n = 3$), * $P < 0.05$, ** $P < 0.01$, and *** $P < 0.001$. C-Cas: cleaved-caspase 3; P-Cas: pro-caspase 3; GAPDH: glyceraldehyde-3-phosphate dehydrogenase.

the C1/Cisplatin group showed significant nuclear shrinkage and fragmentation, indicating extensive cell death (Fig. 9F). These findings were consistent with the TUNEL detection results (Figs. 9G and H). In addition, the WB and immunohistochemical analysis results also confirmed that C1/Cisplatin exhibited a stronger ability to induce mitochondrial apoptosis compared with C1 or Cisplatin alone by regulating the expression of mitochondrial apoptosis and Cisplatin resistance-related proteins (Bax, C-caspase 3 and Cyto C up-regulation, Bcl-2 and GST down-regulation) *in vivo* (Figs. 9I and S16).

Next, the biosafety of combinational therapy was evaluated in healthy BALB/c mice. As opposed to Cisplatin, which significantly

damaged the liver and kidney function of mice, the combined strategy revealed no obvious damage to any major organs, indicating low hepatotoxicity and nephrotoxicity (Fig. S17). Blood panel analysis further demonstrated normal red blood cell (RBC), hemoglobin (HGB), hematocrit (HCT), mean corpuscular volume (MCV), mean corpuscular hemoglobin concentration (MCHC), red blood cell distribution width (RDW), alanine aminotransferase (ALT), aspartate aminotransferase (AST), creatinine (CRE), and blood urea nitrogen (BUN) levels in mice subjected to the combined treatment (Fig. S17). Collectively, these results demonstrate that C1 could effectively enhance Cisplatin sensitivity and anti-HCC efficacy with good biocompatibility *in vivo*.

4. Conclusions

In summary, a smart and simple pyrimidine PM was designed as a “weapon” to identify ideal GST inhibitors, simultaneously monitoring the ability of inhibitors to regulate GST levels *in vitro* and *in vivo*. Considering the elevated levels of GST in blood samples of HCC patients, GST inhibitors could serve as GST-targeting drugs for sensitizing HCC therapy in clinical practice. Notably, the natural compound C1 was screened as a broad “green” GST inhibitor, which effectively down-regulated GST levels and enabled the selective elimination of HCC cells (HepG2 and HepG2/DDP) while showing adequate safety to HL-7702. More importantly, C1 showed a sensitizing anti-HCC effect of Cisplatin in HepG2/DDP cells and *in vivo*. The natural PM exhibited broad GST inhibitory effect, the low toxicity to normal cells, and sensitization to the anti-HCC effect of Cisplatin. Therefore, C1 might be an excellent “green” natural GST inhibitor to enhance sensitivity for Cisplatin in HCC therapy.

CRedit author statement

Linxi Mao: Project implementation, Methodology, Validation, Formal analysis, Investigation, Data curation, Visualization; **Yan Qin:** Project design and implementation, Conceptualization, Methodology, Validation, Formal analysis, Investigation, Data curation, Visualization, Guidance providing, Writing - Original draft preparation; **Jialong Fan:** Validation, Formal analysis; **Weiyang:** Language polishing; **Bin Li and Liang Cao:** Natural compounds extracting and purifying; **Liqin Yuan:** Provision of clinical blood samples; **Mengyun Wang:** Natural compounds extracting and purifying; **Bin Liu:** Conceptualization, Methodology, Validation, Formal analysis, Investigation, Data curation, Visualization, Guidance providing, Writing - Reviewing and Editing; **Weiyang:** Resources, Conceptualization, Methodology, Validation, Formal analysis, Investigation, Data curation, Visualization, Funding acquisition, Project administration.

Declaration of competing interest

The authors declare that there are no conflicts of interest.

Acknowledgments

This work was supported by the National Natural Science Foundation of China (Grant Nos.: 82003931, 82204766 and 81374062), the Outstanding Youth Foundation of Hunan Provincial Education Department of China (Grant No.: 20B445), the Hunan Youth Science and Technology Innovation Talents Project (Grant No.: 2021RC3100), the Chinese Postdoctoral Science foundation (Grant No.: 2021M690974), Changjiang Scholars Program in Ministry Education, People's Republic of China (Program No.: T2019133), and the Scientific Research Project of Hunan Provincial Education Department (Project No.: 21B0394).

Appendix A. Supplementary data

Supplementary data to this article can be found online at <https://doi.org/10.1016/j.jpha.2023.12.013>.

References

- [1] D.A. Fennell, Y. Summers, J. Cadranel, et al., Cisplatin in the modern era: The backbone of first-line chemotherapy for non-small cell lung cancer, *Cancer Treat. Rev.* 44 (2016) 42–50.
- [2] W.S. Li, W.S. Lam, K.C. Liu, et al., Overcoming the drug resistance in breast cancer cells by rational design of efficient glutathione S-transferase inhibitors, *Org. Lett.* 12 (2010) 20–23.
- [3] B. Niu, Y. Zhou, K. Liao, et al., “Pincer movement”: Reversing cisplatin resistance based on simultaneous glutathione depletion and glutathione S-transferases inhibition by redox-responsive degradable organosilica hybrid nanoparticles, *Acta Pharm. Sin.* B 12 (2022) 2074–2088.
- [4] G. Housman, S. Byler, S. Heerboth, et al., Drug resistance in cancer: An overview, *Cancers* 6 (2014) 1769–1792.
- [5] F. Huang, S. Li, X. Lu, et al., Two glutathione S-transferase inhibitors from *Radix angelicae sinensis*, *Phytother. Res.* 25 (2011) 284–289.
- [6] M.G. Bolton, O.M. Colvin, J. Hilton, Specificity of isozymes of murine hepatic glutathione S-transferase for the conjugation of glutathione with L-phenylalanine mustard, *Cancer Res.* 51 (1991) 2410–2415.
- [7] T. Geib, C. Lento, D.J. Wilson, et al., Liquid chromatography-tandem mass spectrometry analysis of acetaminophen covalent binding to glutathione S-transferases, *Front. Chem.* 7 (2019), 558.
- [8] J. Lobo, C. Jerónimo, R. Henrique, Cisplatin resistance in testicular germ cell tumors: Current challenges from various perspectives, *Cancers* 12 (2020), 1601.
- [9] H. Zhang, J. Liu, Y. Sun, et al., Carbon-dipyrrromethenes: Bright cationic fluorescent dyes and potential application in revealing cellular trafficking of mitochondrial glutathione conjugates, *J. Am. Chem. Soc.* 142 (2020) 17069–17078.
- [10] A. Chatterjee, S. Gupta, The multifaceted role of glutathione S-transferases in cancer, *Cancer Lett.* 433 (2018) 33–42.
- [11] A. Sau, F. Pellizzari Tregno, F. Valentino, et al., Glutathione transferases and development of new principles to overcome drug resistance, *Arch. Biochem. Biophys.* 500 (2010) 116–122.
- [12] Y. Musdal, U.M. Hegazy, Y. Aksoy, et al., FDA-approved drugs and other compounds tested as inhibitors of human glutathione transferase P1-1, *Chem. Biol. Interact.* 205 (2013) 53–62.
- [13] T. Ertan-Bolelli, Y. Musdal, K. Bolelli, et al., Synthesis and biological evaluation of 2-substituted-5-(4-nitrophenyl)sulfonamido/benzoxazoles as human GST P1-1 inhibitors, and description of the binding site features, *ChemMedChem* 9 (2014) 984–992.
- [14] M. Pasello, F. Michelacci, I. Scloniti, et al., Overcoming glutathione S-transferase P1-related cisplatin resistance in osteosarcoma, *Cancer Res.* 68 (2008) 6661–6668.
- [15] F. Pellizzari Tregno, A. Sau, S. Pezzola, et al., *In vitro* and *in vivo* efficacy of 6-(7-nitro-2, 1, 3-benzoxadiazol-4-ylthio)hexanol (NBDHEX) on human melanoma, *Eur. J. Cancer* 45 (2009) 2606–2617.
- [16] M. Pasello, M.C. Manara, F. Michelacci, et al., Targeting glutathione-S transferase enzymes in musculoskeletal sarcomas: A promising therapeutic strategy, *Anal. Cell. Pathol. (Amst)* 34 (2011) 131–145.
- [17] P. Turella, C. Cerella, G. Filomeni, et al., Proapoptotic activity of new glutathione S-transferase inhibitors, *Cancer Res.* 65 (2005) 3751–3761.
- [18] P. Turella, G. Filomeni, M.L. Dupuis, et al., A strong glutathione S-transferase inhibitor overcomes the P-glycoprotein-mediated resistance in tumor cells, *J. Biol. Chem.* 281 (2006) 23725–23732.
- [19] G. Filomeni, P. Turella, M.L. Dupuis, et al., 6-(7-Nitro-2, 1, 3-benzoxadiazol-4-ylthio)hexanol, a specific glutathione S-transferase inhibitor, overcomes the multidrug resistance (MDR)-associated protein 1-mediated MDR in small cell lung cancer, *Mol. Cancer Ther.* 7 (2008) 371–379.
- [20] L. Tentori, A.S. Dorio, E. Mazzone, et al., The glutathione transferase inhibitor 6-(7-nitro-2, 1, 3-benzoxadiazol-4-ylthio)hexanol (NBDHEX) increases temozolomide efficacy against malignant melanoma, *Eur. J. Cancer* 47 (2011) 1219–1230.
- [21] A. De Luca, F. Pellizzari Tregno, A. Sau, et al., Glutathione S-transferase P1-1 as a target for mesothelioma treatment, *Cancer Sci.* 104 (2013) 223–230.
- [22] L. Federici, C. Lo Sterzo, S. Pezzola, et al., Structural basis for the binding of the anticancer compound 6-(7-nitro-2, 1, 3-benzoxadiazol-4-ylthio)Hexanol to human glutathione S-transferases, *Cancer Res* 69 (2009) 8025–8034.
- [23] W.H. Ang, I. Khalaila, C.S. Allardyce, et al., Rational design of platinum(IV) compounds to overcome glutathione-S-transferase mediated drug resistance, *J. Am. Chem. Soc.* 127 (2005) 1382–1383.
- [24] K.G.Z. Lee, M.V. Babak, A. Weiss, et al., Development of an efficient dual-action GST-inhibiting anticancer platinum(IV) prodrug, *ChemMedChem* 13 (2018) 1210–1217.
- [25] M. Won, S. Koo, H. Li, et al., An ethacrynic acid-brominated BODIPY photosensitizer (EA-BPS) construct enhances the lethality of reactive oxygen species in hypoxic tumor-targeted photodynamic therapy, *Angew. Chem. Int. Ed.* 60 (2021) 3196–3204.
- [26] Y. Qin, C. Peng, W. Yang, et al., A bi-functional fluorescent probe for visualized and rapid natural drug screening via GSTs activity monitoring, *Sens. Actuat. B* 328 (2021), 129047.
- [27] M. Mendes, B. Pamplona, S. Kumar, et al., Ion-pair formation in neutral potassium-neutral pyrimidine collisions: Electron transfer experiments, *Front. Chem.* 7 (2019), 264.
- [28] C. Lu, W. Lin, W. Wang, et al., Kinetic observation of rapid electron transfer between pyrimidine electron adducts and sensitizers of riboflavin, flavin adenine dinucleotide (FAD) and chloranil: A pulse radiolysis study, *Radiat. Phys. Chem.* 59 (2000) 61–66.
- [29] X. Liu, L. Chen, Q. Zhou, et al., Electron transfer reactions between 1, 8-dihydroxyanthraquinone and pyrimidines: A laser flash photolysis study, *J. Photochem. Photobiol. A* 269 (2013) 42–48.
- [30] J. Chen, G. Wang, X. Su, Fabrication of red-emissive ZIF-8@QDs nanoprobe with improved fluorescence based on assembly strategy for enhanced biosensing, *Sens. Actuat. B* 368 (2022), 132188.

- [31] X. Zhou, M. Wang, X. Su, Sensitive glutathione S-transferase assay based on Fe-doped hollow carbon nanospheres with oxidase-like activity, *Sens. Actuat. B* 338 (2021), 129777.
- [32] L. Qin, X. He, L. Chen, et al., Turn-on fluorescent sensing of glutathione S-transferase at near-infrared region based on FRET between gold nanoclusters and gold nanorods, *ACS Appl. Mater. Interfaces* 7 (2015) 5965–5971.
- [33] H. Chen, X. Yang, Y. Liu, et al., Turn-on detection of glutathione S-transferase based on luminescence resonance energy transfer between near-infrared to near-infrared core-shell upconversion nanoparticles and organic dye, *Anal. Bioanal. Chem.* 412 (2020) 5843–5851.
- [34] L.R. Kelland, Preclinical perspectives on platinum resistance, *Drugs* 59 (2000) 1–8, discussion 37–38.
- [35] Y. Qin, M. Daniyal, W. Wang, et al., An enhanced silver nanocluster system for cytochrome c detection and natural drug screening targeted for cytochrome C, *Sens. Actuat. B* 291 (2019) 485–492.